

# The phase-space of boxy-peanut and X-shaped bulges in galaxies

## II. The relation between face-on and edge-on boxiness

P.A. Patsis,<sup>1,2\*</sup> M. Katsanikas,<sup>1†</sup>

<sup>1</sup>Research Center for Astronomy, Academy of Athens, Soranou Efessiou 4, GR-115 27, Athens, Greece

<sup>2</sup>Excellence Cluster Universe, Boltzmannstr. 2, D-85748, Garching, Germany

Accepted .....Received .....in original form .....

### ABSTRACT

We study the dynamical mechanisms that reinforce the formation of boxy structures in the *inner* regions, roughly in the middle, of bars observed nearly *face-on*. Outer boxiness, at the ends of the bars, is usually associated with orbits at the inner, radial 4:1 resonance region and can be studied with 2D dynamics. However, in the middle of the bar dominate 3D orbits that give boxy/peanut bulges in the edge-on views of the models. In the present paper we show that 3D quasi-periodic, as well as 3D chaotic orbits sticky to the  $x1v1$  and  $x1v1'$  tori, especially from the Inner Lindblad Resonance (ILR) region, have boxy projections on the equatorial plane of the bar. The majority of vertically perturbed 2D orbits, initially on the equatorial plane in the ILR resonance region, enhance boxy features in face-on bars. Orbits that build a bar by supporting sharp “X” features in their side-on views at energies *beyond* the ILR, may also have a double boxy character. If populated, the extent of the inner boxiness along the major axis is about the same with that of the peanut supporting orbits in the side-on views. At any rate these orbits do not obscure the observation of the boxy orbits of the ILR region in the face-on views, as they contribute more to the surface density at the sides of the bar than to their central parts.

**Key words:** Galaxies: kinematics and dynamics – chaos – diffusion structure

### 1 INTRODUCTION

Boxiness of galactic bulges is in most cases discussed in connection with the boxiness observed in the edge-on views of disc galaxies. However, boxiness is encountered also in nearly face-on views of barred galaxies. This can be either an overall boxiness of the bar, usually referring to rectangularity of the outermost isophotes of the bar component in early-type barred galaxies (see e.g. Ohta et al. 1990), or boxiness of the isophotes in the inner regions, i.e. in distances from the centre roughly up to the middle of the semi-major axis of the bar (Erwin & Debattista 2013).

As regards the outer boxiness it is plausible to assume that it is related with orbits at the end of the bar, i.e. at regions with a much smaller scale height than that of the regions of the bar that participate in the formation of the peanut. In that respect, for the outer boxiness of the bar the presence of the radial 4:1 resonance brings in the system rectangular-like p.o. (Contopoulos 1988) that attract around them quasi-periodic or sticky non-periodic orbits. The role of chaotic orbits in reinforcing the outer boxiness of the bars has been indicated by Wozniak (1994), Kaufmann & Contopoulos (1996), Patsis et al. (1997) and Wozniak & Pfenniger (1999). This can lead to the boxy shapes of early type bars. In the study of the

outer face-on boxiness of the bars, we deal practically with 2D dynamics. Thus, we find in 2D models, that orbits associated with this feature are also related with the orbits building the chaotic spirals beyond corotation (Patsis 2006; Tsigaridi & Patsis 2013), i.e. both structures share the same orbital content. Essentially these are orbits on the equatorial plane. Nevertheless, the connection of the rectangularity of a bar with the radial 4:1 resonance has been also detected in 3D models (Patsis et al. 2003). However, the relevant orbits remain at small heights away from the equatorial plane.

For the *inner* boxiness on the other hand we must use 3D orbits. If we accept the dimensions of a boxy bulge being as discussed in Patsis & Katsanikas (2014) (hereafter paper I), the rectangularity of the inner isophotes (as depicted in the figures of Erwin & Debattista 2013) corresponds to regions occupied by the b/p bulge in the side-on profiles. From this arises the question if there exist 3D orbits contributing both to a face-on as well as to a side-on boxy profile. The existence of this combination is not obvious. Thinking about the shapes of periodic orbits, or about quasi-periodic orbits with similar shapes like the periodic ones, this combination does not exist neither for this model nor for any other of the models in Skokos et al. (2002a,b) or in the model used by Katsanikas & Patsis (2011). The periodic orbits of the  $x1$ -tree ( $x1$ ,  $x1v1$ ,  $x1v2$ ,  $x1v3$  etc.) follow in their projections on the equatorial plane the morphological evolution of the  $x1$  family as the Jacobi constant (hereafter called energy) increases. We have to reach en-

\* patsis@academyofathens.gr (PAP)

† mkatsan@academyofathens.gr (MK)

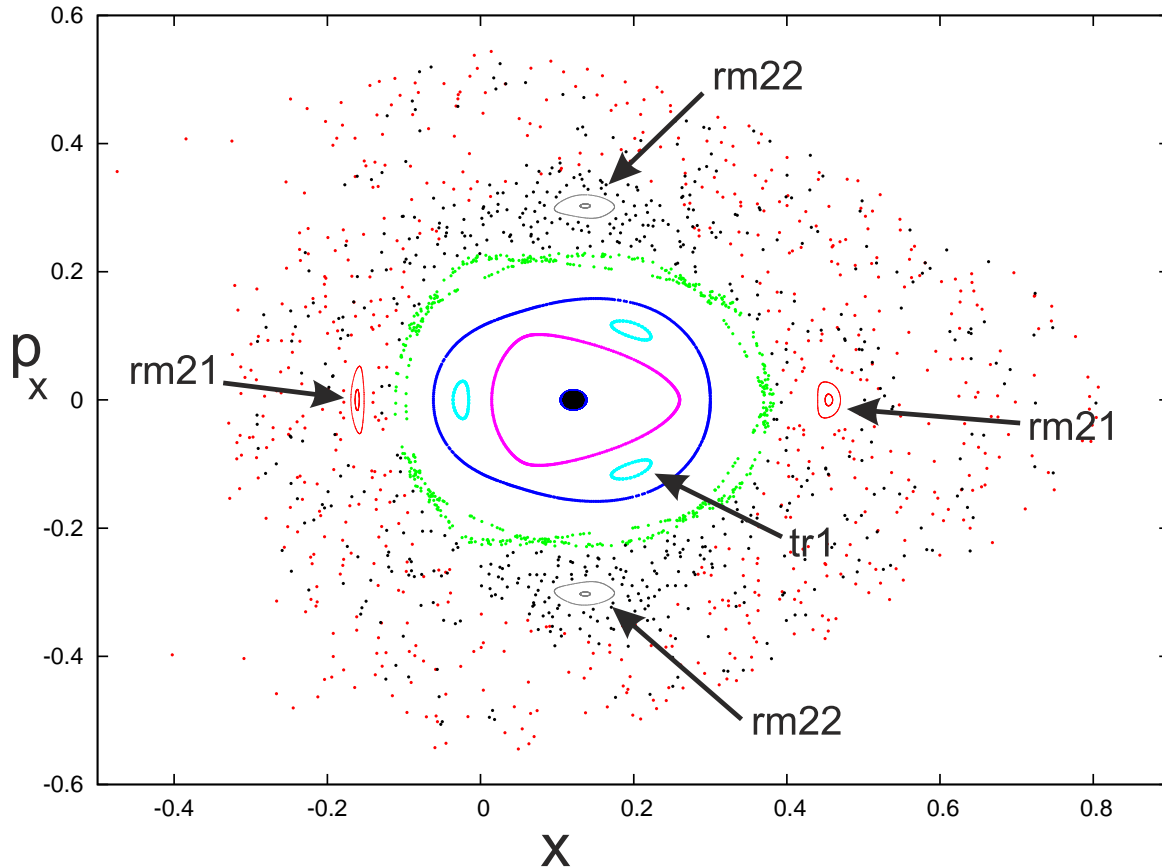


**Figure 1.** The  $(x, p_x)$  cross section at  $E_J = -0.41$ , constructed by perturbing the  $x_1$  initial conditions by  $\Delta x$  (see text). The important for the dynamics of our model families of multiplicity 2  $rm21$  and  $rm22$ , as well as the family  $tr1$ , of multiplicity 3, are indicated with arrows. In this diagram the initial conditions of  $x_1$ ,  $x_{1v1}$ ,  $x_{1v2}$  and  $x_{1mul2}$  almost overlap at about  $(x, p_x) = (0.1, 0)$  (heavy black dot).

ergies at the radial 4:1 resonance in order to obtain a rectangular shape in their face-on,  $(x, y)$  in our model, projection (Contopoulos 1983). Orbits with such energies are found in the outer parts of the bars. However, if we consider large  $\Delta z$  or  $\Delta p_z$  perturbations of planar p.o. in the 4:1 resonance region, calculating in this way orbits with large  $|z|$  values, we enter into chaotic regimes of the models, where orbits do not support any particular structure. By excluding orbits with large energies, i.e. at or between the radial 4:1 resonance and corotation, we have to seek after orbits in lower energies, where we encounter the orbits supporting the boxiness of the edge-on profiles. Stable 2D orbits of the planar, “3:1-type”, families could contribute to the reinforcement of boxy structures on the equatorial plane (Patsis et al. 2003). Vertically perturbed orbits with  $(x_0, p_{x_0})$  initial conditions on their islands of stability are candidates for providing 3D orbits with boxy projections on the  $(x, y)$  plane. This possibility has to be examined for representatives of these families with appropriate energies. We already have seen that there are orbits supporting the side-on b/p bulge without having a “ $x_1$ -like” morphology in their face-on projection (cf figure 19 in paper I). In the present paper we examine the possibility of having among them orbits with boxy  $(x, y)$  projections.

We use in our work the same model as in paper I and we keep the same formalism. In section 2, starting with 2D orbits on the equatorial plane, we examine their orbital behaviour when they are perturbed away from it. Focusing on the non-periodic orbits that support the b/p structure we first study their dynamics in the typi-

cal case where all important families coexist and  $x_1$  is stable. Then we investigate as well possible changes introduced in the energy interval of the vertical ILR, where  $x_1$  is simple unstable. In section 3 we investigate the role of symmetric orbits bifurcated at odd, radial  $n:1$  resonances. Finally, we summarise our results and discuss our conclusions in section 4.

## 2 3D ORBITS WITH BOXY FACE-ON PROJECTIONS

### 2.1 Dynamics at a typical energy

An energy at which all main families of p.o. contributing to the b/p structure coexist is  $E_J = -0.41$ . At this energy  $x_1$ ,  $x_{1v1}$  and  $x_{1mul2}$  are stable, while  $x_{1v2}$  is simple unstable (Skokos et al. 2002a; Patsis & Katsanikas 2014). It is a typical energy for understanding the dynamics at the peanut region.

#### 2.1.1 $x_1$ perturbations by $\Delta x$

We examine the contribution of non-periodic orbits in the neighbourhood of p.o. from these four families to the reinforcement of inner boxy features, first by successively perturbing the  $x_1$  p.o. by increasing  $p_x$ . Fig. 1 gives the  $(x, p_x)$  cross section at  $E_J = -0.41$ , which has been constructed this way. We investigate the phase space occupied by these orbits, when they are kicked out of the

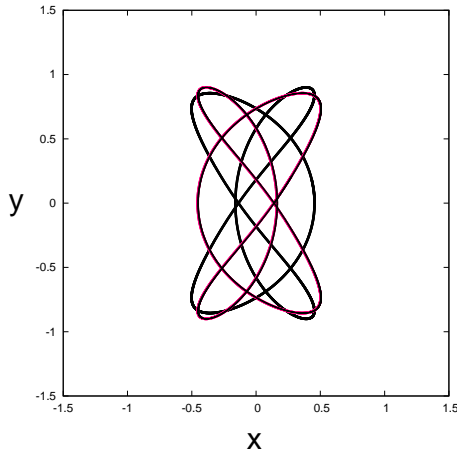


**Figure 2.** The morphology of the two planar simple unstable p.o. rm21 and rm22 (black and magenta) at  $E_J = -0.41$ .

equatorial plane. In the  $(x, p_x)$  cross section the initial conditions of all important families of p.o. involved in the enhancement of the boxy side-on profiles, i.e.  $x1$ ,  $x1v1$ ,  $x1v2$  and  $x1mul2$ , almost overlap at about  $(x, p_x) = (0.1, 0)$ . Their location is indicated with a heavy black dot in Fig. 1. In the same figure we observe that the perturbed  $x1$  orbits form around the p.o. a large central region, characterized mainly by order. Inside this stability island we discern three smaller stability islands belonging to a p.o. of multiplicity 3, let us call it  $tr1$ , and further out a chain of seven stability islands (drawn with green) that mark the border between the ordered region and a chaotic zone that surrounds it. Embedded in this chaotic zone we observe two sets of islands. They are related to two p.o. of multiplicity 2, which we name  $rm21$  and  $rm22$  and are centred at  $(x, p_x) \approx (0.137, \pm 0.3)$  and  $(0.455 / -0.16, 0)$  respectively. Arrows in Fig. 1 indicate the locations of the orbits  $tr1$ ,  $rm21$  and  $rm22$ . Other families of p.o. existing at this energy, like  $x2$  and  $x3$ , are not discussed at this point and are not indicated in Fig. 1. By inspection of Fig. 1 these three families of higher multiplicity seem to play a minor role in the enhancement of any morphological feature in the model. However, our investigation has shown the opposite, so we present here in detail how they contribute to the enhancement of boxiness in both face-on and side-on views.

The families  $rm21$  and  $rm22$  have morphologies symmetric with respect to the  $y = 0$  axis. They are given together in Fig. 2, with black and magenta colours respectively. The combination of the two p.o. provide a morphology ideal for supporting boxy structures in the central parts of face-on bars, first of all on the equatorial plane. Even so, the system should provide for that purpose also non-periodic orbits that will follow similar morphologies. In order to trace the origin of the  $rm21$  and  $rm22$  families we plot the stability diagram of  $x1$  considering it as being of multiplicity two (Fig. 3). Both  $rm21$  and  $rm22$  families have the same stability indices, as they are essentially two branches of one family, symmetric with respect to the  $x = 0$  axis. They are bifurcated from  $x1$  at  $E_J \approx -0.435$ , where the  $b1$  stability index of  $x1$ , considered as being of multiplicity 2, has a tangency with the  $b = -2$  axis. The  $b1$  stability index is associated with radial perturbations, so two 2D families of p.o. are bifurcated. They are initially simple unstable (U), since the mother family  $x1$  is U at the energy they are introduced in the system.

The other family of higher multiplicity we have encountered

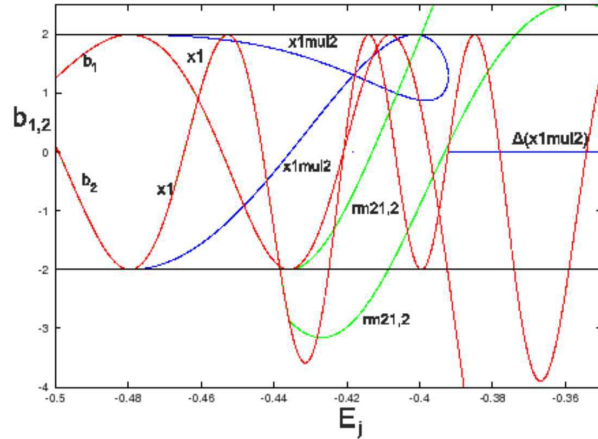


**Figure 3.** The red curves give the evolution of the stability indices of the  $x1$  family when it is considered being of multiplicity 2. The family  $x1mul2$  is introduced in the system at  $E_J \approx -0.479$ .

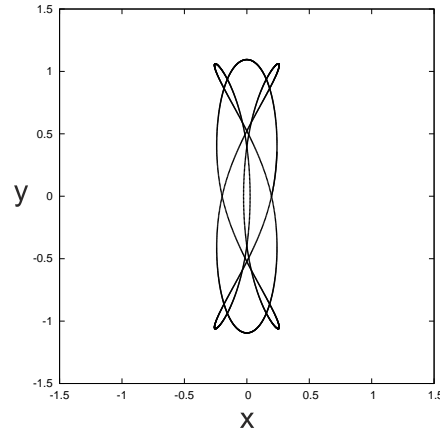


**Figure 4.** The stable family of multiplicity 3,  $tr1$ , at  $E_J = -0.41$ .

at  $E_J = -0.41$  is the orbit of multiplicity 3,  $tr1$ , which is indicated with an arrow, inside the territory of the central stability island in Fig. 1. It coexists together with its unstable counterpart of multiplicity 3, which is located between the three islands of stability (not indicated in Fig. 1). The origin of  $tr1$  can be found by considering it as a “deuxième genre” family (Poincaré 1899). Since it is a radial bifurcation of  $x1$  its starting point has to be sought at an energy where the corresponding stability index of the simple periodic mother family will be  $b = -2 \cos(\frac{2\pi}{3}) = 1$  (see e.g. the appendix in Skokos et al. 2002b). This happens for  $E_J \approx -0.4617$  (cf figure 1b in paper I).

### 2.1.2 Vertical perturbations of planar orbits on “invariant curves”

At  $E_J \approx -0.4617$   $tr1$  is bifurcated from  $x1$  as stable and extends over a significant range of energies, including the ILR region, until it becomes simple unstable at  $E_J \approx -0.4039$ . Its face-on portrait is boxy, as can be seen in Fig. 4. In addition its stability secures motion on 4D tori and sticky orbits on them. Perturbations up to  $\Delta z = 0.04$  of orbits starting on the  $(x, p_x)$  plane in the region be-

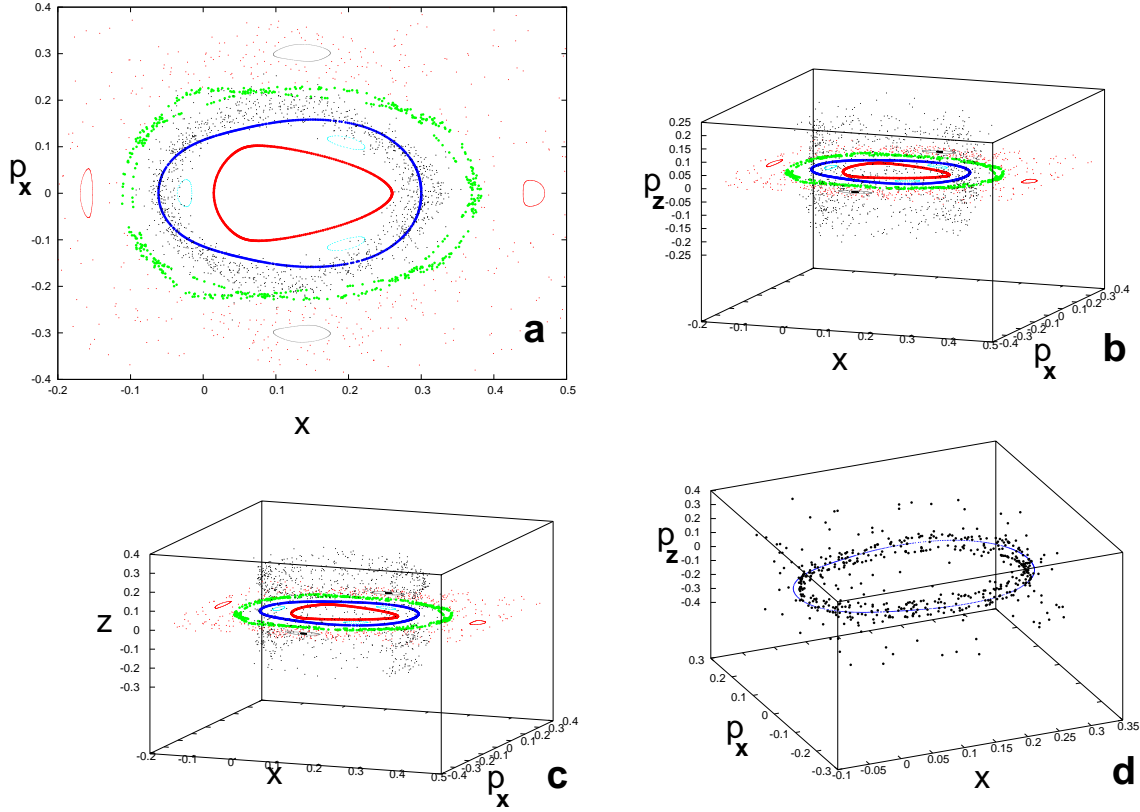


**Figure 5.** (a) The ring of black consequents projected in the region of the island of stability in the  $(x, p_x)$  plane is formed by an orbit starting on a closed curve around rm21. It stays trapped in this zone for 850 periods of  $x1$  ( $E_j = -0.41$ ). In (b) we give the 3D  $(x, p_x, p_z)$  and in (c)  $(x, p_x, z)$  projections of the space of section with the same orbits. We observe that the consequents forming the ring in (a) stay confined in cylindrical structures among the invariant curves of the central stability island of the  $(x, p_x)$  plane in (a). In (d) we observe that also an orbit with a small deviation in its initial conditions from the first one has a qualitatively similar behaviour.

tween the dark blue and red coloured invariant curves in Fig. 1 give orbits on triple rotational tori. The face-on morphologies of these orbits can be thought as thick versions of the tr1 p.o. as depicted in Fig. 4. Their side-on projections have a b/p profile, however they remain close to the equatorial plane, reaching heights  $|z| \lesssim 0.08$ . Quasi-periodic orbits found by adding  $p_{z0} \neq 0$  to the orbits on the invariant curves in the  $(x, p_x)$  plane give orbital morphologies similar to those we find when we impose  $\Delta z$  perturbations with slightly thicker side-on views.

The closed elliptical curves around rm21 and rm22 indicate stability only on the equatorial plane. However, these families are at  $E_j = -0.41$  unstable to vertical perturbations ( $b_2 = -2.15$ ) and thus non-periodic orbits in their neighbourhood in the  $z$  or  $p_z$  directions will be chaotic. Even very small  $\Delta z$  or  $\Delta p_z$  perturbations of an orbit on an invariant curve around rm21 or rm22, bring the perturbed orbits away from the  $(x, p_x)$  plane. Nevertheless, we observe that these orbits during their integration stay confined in some regions of the 4D space of section. As an example we consider an orbit starting on an invariant curve around rm21 with  $(x_0, p_{x0}) = (0.47, 0)$ , which is perturbed by  $p_z = 0.03$ . We integrated it for time equal to 2000  $x1$  periods having an energy conservation with a relative error less than  $10^{-15}$ . For time corresponding to 10  $x1$  periods this orbit stays outside the region defined by the seven stability islands in Fig. 1. Then its consequents are found inside the seven islands region and they are projected in

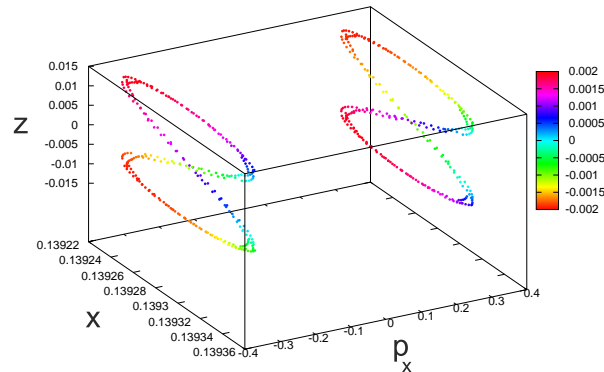


**Figure 6.** The 4D structure of a double tube torus around rm22. The self-intersections of the “8”-shaped structures is a projection effect, since the two branches have different colours (colours are according to the  $p_z$  values at the right hand side).

the  $(x, p_x)$  plane around the blue invariant curve. They stay there forming a ring for more than 850  $x1$  orbital periods. This is the ring of black points that can be observed in Fig. 5a close and around the blue invariant curve region.

The formation of a ring structure in the  $(x, p_x)$  plane corresponds to a spatial confinement of the orbits in both 3D projections of the 4D space of section, which include this plane, namely  $(x, p_x, p_z)$  and  $(x, p_x, z)$ . In both of these two 3D projections we have the formation of a cylindrical structure that extends away from the  $(x, p_x)$  plane remaining surrounded by the chain of the seven stability islands. This can be seen in Fig. 5b and Fig. 5c for the  $(x, p_x, p_z)$  and  $(x, p_x, z)$  projections respectively. 3D projections including the  $(z, p_z)$  plane are very illustrative for understanding the dynamical character of these orbits and are described below extensively. For the time being we want to underline that despite their sticky character these orbits are chaotic. In the example of the orbit we describe, this means,

(i) that if we extend the integration time, the consequents of the orbit will cross again the border of the seven stability islands on the  $(x, p_x)$  projection and will diffuse in a larger volume of the phase space. Nevertheless, later they return and stay trapped on the area of the ring of Fig. 5a for hundreds of  $x1$  dynamical times. Also during the time an orbit spends away from a sticky zone, i.e. in the example of our orbit away from the ring, it may stay confined for a time interval within this period in another subspace of the space of section. In our case the orbit stays for several hundreds of  $x1$  periods confined within the area of the innermost, red, invariant curve in Fig. 5a before it returns again to the ring area and spends another time interval of more than 200  $x1$  periods in this zone.

(ii) that starting at nearby initial conditions we will have a qualitatively different orbital behaviour. Nevertheless *qualitatively* the overall dynamical behaviour is similar. If we add a tiny  $p_{x0} = 10^{-4}$  perturbation to the initial conditions of the orbit with the black consequents in Fig. 5a,b,c we do not find the new orbit being trapped in the same zones of the phase space during the same or close-by time intervals. However, we find it spending time of the same order (hundreds of  $x1$  periods) in roughly the same zone, e.g. the ring area. The trapping of this new orbit in the area around the blue invariant of Fig. 5a is given in Fig. 5d.

### 2.1.3 Vertical perturbations of planar orbits in chaotic seas

This orbital behaviour is typical not only for orbits starting on the invariant curves of rm21 and rm22 in the  $(x, p_x)$  plane, but for all orbits we started integrating from the “chaotic sea” region of Fig. 1. This is to be expected since essentially we deal with a single chaotic sea. In infinite time a chaotic orbit will visit the whole available volume of the phase space. However here, we integrate parts of this orbit starting from different initial conditions. Even in the region  $-0.409 < E_J < -0.4$ , where rm21, rm22 are stable (Fig. 3) the above orbital dynamics does not practically change, because the zone of influence around these stable p.o. is small. In this case we have found a double “tube torus” (i.e. a self-intersecting torus in a 3D projection, see Vrahatis et al. 1997) in the 4D phase space. We present it in Fig. 6 at  $E_J = -0.4084$  since it is the first time we find a tube torus in a family of higher multiplicity. The tori belong to the perturbed by  $\Delta p_z = 0.001$  rm22 orbit at that energy. The formed “ribbons” have an intersection in the 3D  $(x, p_x, z)$  projection, but not in the 4D space as one concludes from the different colours (according to the  $p_z$  coordinate) of the intersecting branches. For slightly larger perturbations of the stable p.o. in the  $p_z$  or  $z$  directions the orbits diffuse in phase space. It is evident that the orbits originating in the chaotic sea around the central stability region in the  $(x, p_x)$  cross section (Fig. 5a) represent a major class of orbits, since they occupy a large volume of the phase space and have similar behaviour in the

examined range of energies  $-0.435 < E_J < -0.375$ . So, we want to investigate if there is a particular group among them contributing to boxy structures in their face-on views. Their  $E_J$  values point to the right size of orbits for supporting the inner boxiness we study. If so, we want also to find out what is the common feature of such an orbital set. For example we want to investigate if they reinforce boxy face-on structures when they stay at a particular region of the phase space.

The first thing that we have examined is whether the orbit we have studied starting on the invariant curve of rm21 on the  $(x, p_x)$  plane, supports a particular morphology during the time it spends in the ring inside the chain of the seven stability islands. The result is striking as can be seen in Fig. 7. In Fig. 7a we observe that the face-on projection has clearly a boxy character. Since the orbit stays in the ring for more than 850  $x1$  periods we sample it every 100 points during this time interval in order to plot Fig. 7a. The dimensions of the box are comparable with the dimensions of the tr1 p.o. in Fig. 4. Simultaneously, we observe that the side-on,  $(y, z)$ , projection of the orbit (Fig. 7b) reflects the morphology of orbits trapped around  $x1v1$  and  $x1v1'$ , since it appears as a combination of “ $\smile$ ” and “ $\frown$ ” parts. We already know the imprint of sticky chaotic orbits to the tori of these families in the  $(z, p_z)$  plane from paper I (cf figure 14 in paper I). The spreading of the consequents of the orbit during the time of the 850  $x1$  periods in the  $(z, p_z)$  reproduces exactly this typical pattern, as we can observe in Fig. 7c.

We have already seen that during the time an orbit forms a ring of consequents projected inside the area defined by the chain of the seven stability islands in the  $(x, p_x)$  plane, it can support an inner boxy feature in the face-on view of the model. Next, as a second step, we examine if we have a similar behaviour in the case of orbits having projected consequents during their integration time only in the chaotic zone of Fig. 1. Such orbits exist indeed. As an example we give the orbit with initial conditions  $(x_0, z_0, p_{x_0}, p_{z_0}) = (0.515, 0.034, 0, 0)$ , always at the typical energy  $E_J = -0.41$ . For time corresponding to about 300  $x1$  periods, its face-on morphology has a boxy character with dimensions similar to the combined rm21,2 p.o. (Fig. 2). This is given in Fig. 8a. With black we depict the orbit integrated for 10 periods of  $x1$ , while the red background depicts the same orbit integrated for 300  $x1$  periods. The side-on morphology can be observed in Fig. 8b and it is boxy. Although not as sharp as the one in Fig. 7b, this orbit has again a morphology similar to the one produced by a combination of quasi-periodic orbits around  $x1v1$  and  $x1v1'$ . It has an overall b/p morphology and it reaches heights close to  $|z| = 0.4$ . Let us call “phase A” the time interval corresponding to 300  $x1$  periods within which the orbit has the morphology presented in Figs. 8a and 8b. For time larger than 300  $x1$  periods, the morphology of the orbit changes in a characteristic way and is given in Figs. 8c and 8d. The red background corresponds now to the part of the orbit in the time interval between 300 and 1000  $x1$  periods after starting the integration. We call this period “phase B”. With black we plot the orbit during the first 12  $x1$  periods during “phase B”. The face-on view (Figs. 8c) becomes rounder but evidently it increases the surface density in two stripes parallel to the  $y$ -axis at  $x \approx \pm 0.35$ . They can be better seen in the red background and are indicated with arrows. In the side-on view of the orbit (Fig. 8d) we realize that the denser stripes parallel to the  $y$ -axis are like two caps, that restrict the extent of the orbit to  $|z| \gtrsim 0.4$ . In intermediate heights the orbit does not follow any particular morphology.

The consequents of the orbit in Fig. 8 remain projected *around* the central stability island of the  $(x, p_x)$  plane (Fig. 1). Practically they overlap with the chaotic sea as depicted in Fig. 1. However,

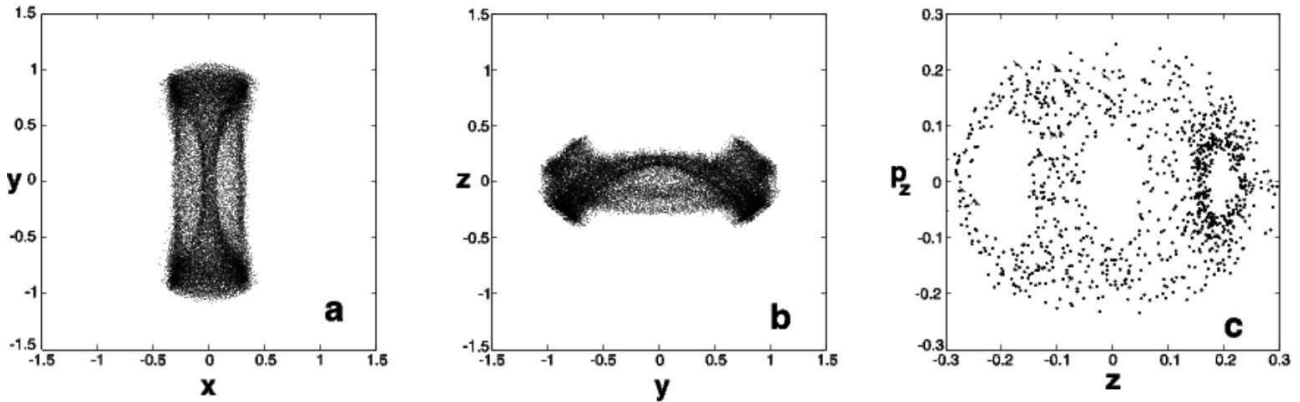


**Figure 7.** The morphology of the chaotic orbit during the time it remains trapped in the ring region of Fig. 5a, is given in (a) (face-on) and (b) (side-on). The  $(z, p_z)$  cross section of this orbit is given in (c). It designates the stickiness of the orbit to the  $x1v1$  and  $x1v1'$  tori.

as we move from “phase A” to “phase B” they drift from the area of the seven stability islands to larger distances. A few consequents during “phase B” are found around the stability island of the planar retrograde family  $x4$ . (The invariant curves around  $x4$  are not drawn in Fig. 1. They are located to the left of the figure, reaching  $x < 0$  values outside the drawn frame). To a large extent the consequents of the orbit in Fig. 8 surround the stability region in Fig. 1 *on the*  $(x, p_x)$  plane forming two vaguely defined successive rings.

#### 2.1.4 The dynamical mechanism

The projections of the consequents of the orbit of our example in the  $(z, p_z)$  plane, are given in Fig. 8e. They are given together with the consequents of a sticky orbit around  $x1v1$  and  $x1v1'$  (magenta dots), as well as together with the projections of the rotational tori of the  $x1mul2$  family at the top and the bottom of the figure around the points  $(z, p_z) = (0.1, \pm 0.42)$  (cf. figure 14 in paper I). The red and the dark blue rings in the central region of the figure are the projections of one of the innermost and one of the outermost tori around  $x1$  respectively. Green points in Fig. 8e are the consequents of the orbit during phase “A”. They start being projected in the  $(z, p_z)$  plane inside the blue ring, but then they move outside it, and occupy roughly the same region with the magenta orbit, which is sticky to  $x1v1$  and  $x1v1'$ . The area covered by the consequents and their distribution on the  $(z, p_z)$  plane are very close also to the projected consequents of the orbit in Fig. 7c. During “phase A” the orbit is unambiguously sticky to  $x1v1$  and  $x1v1'$ . For longer integration times, during “phase B”, the consequents form a ring roughly surrounding the green consequents and are plotted in black. Their relative location during the two different phases “A” and “B”, are given also in the embedded frame in the upper right corner of Fig. 8e. The dimensions of the embedded frame are the same as of the main frame of Fig. 8e. The ring of black points is located practically around the green consequents and its extent in the  $p_z$  direction seems to be hindered by the  $x1mul2$  tori. The weak confinement in two ring structures in the  $(x, p_x)$  and  $(z, p_z)$  planes seems to be enough to secure a boxy character in the configuration space, of the kind described in Fig. 8c and d.

The time intervals of hundreds of  $x1$  dynamical times are already longer than the time needed to consider a structure as supported by orbits. However, following the orbit of Fig. 8 for even longer times gave further interesting results. For time larger than 1000 periods of  $x1$ , the consequents in the  $(z, p_z)$  projection return

inside the dark blue ring and form another ring, this time coloured with grey in Fig. 8e. The consequents remain trapped on this ring for at least 2500  $x1$  periods. By the same time they remain trapped on (rotational) tori around  $x4$  and would be projected to the left of the “chaotic sea” in Fig. 1 (roughly at  $x < -0.2$ ). During this last phase no boxiness is supported in the face-on view of the model. Instead the orbit forms a counter-rotating disk on the  $(x, y)$  plane. In the  $(y, z)$  projection the orbit builds a thick layer close to the equatorial plane, without any particular substructure. Thus, integrated for more than 1000 dynamical times this orbit does not reinforce the double boxy profile. This case offers a counter-example of a sticky orbit reinforcing a structure. Like quasi-periodic orbits being trapped around a “wrong” stable periodic orbit, as is  $x4$  for the building of a galactic bar, during this phase the sticky chaotic orbit destroys the boxy structure in our example. In the case of sticky orbits, our example shows how the same orbit can reinforce or destroy a structure during different phases of its evolution. The information about the trapping around different tori of p.o. can be obtained only directly by means of the method of the surface of section.

Until now it became clear that a large number of planar orbits, which are displaced from the equatorial plane by perturbations in the  $z$  or  $p_z$  directions become sticky to the  $x1v1$  and  $x1v1'$  tori and during this phase they support a double boxy morphology. This happens in the energy interval  $-0.435 < E_J < -0.375$ . However, the time interval during their integration, during which they will be trapped at specific regions of the phase space varies as we change the initial conditions. Immediate support of the double boxiness from the beginning of the integration is obtained by vertically perturbed orbits with  $(x, p_{x_0})$  initial conditions from the region between the dark blue invariant, just beyond the  $tr1$  islands and the orbit of multiplicity 7 in Fig. 1. By perturbing initial conditions in this region in the  $z$  or  $p_z$  direction we find quasi-periodic orbits on 4D tori and orbits sticky to these tori, which have a double-boxy morphology. As a typical example we give the orbit with  $(x_0, z_0, p_{x_0}, p_{z_0}) = (0.3, 0, 0, 0.3)$ . Its face-on and side-on views are given in Fig. 9a,b respectively. With black is given the orbit integrated for 10 periods of  $x1$  at  $E_J = -0.41$ , while with red is the same orbit integrated for 100  $x1$  periods. However, the orbit continues to reinforce the orbit for many hundreds of  $x1$  dynamical times. We observe in Fig. 9b, that the orbit reaches heights  $|z| \approx 0.5$ . The dynamical mechanism is similar to the one we described for the orbits we started integrating in the chaotic sea of Fig. 1, namely stickiness to the tori of  $x1v1$  and  $x1v1'$ . This becomes evident if we look at

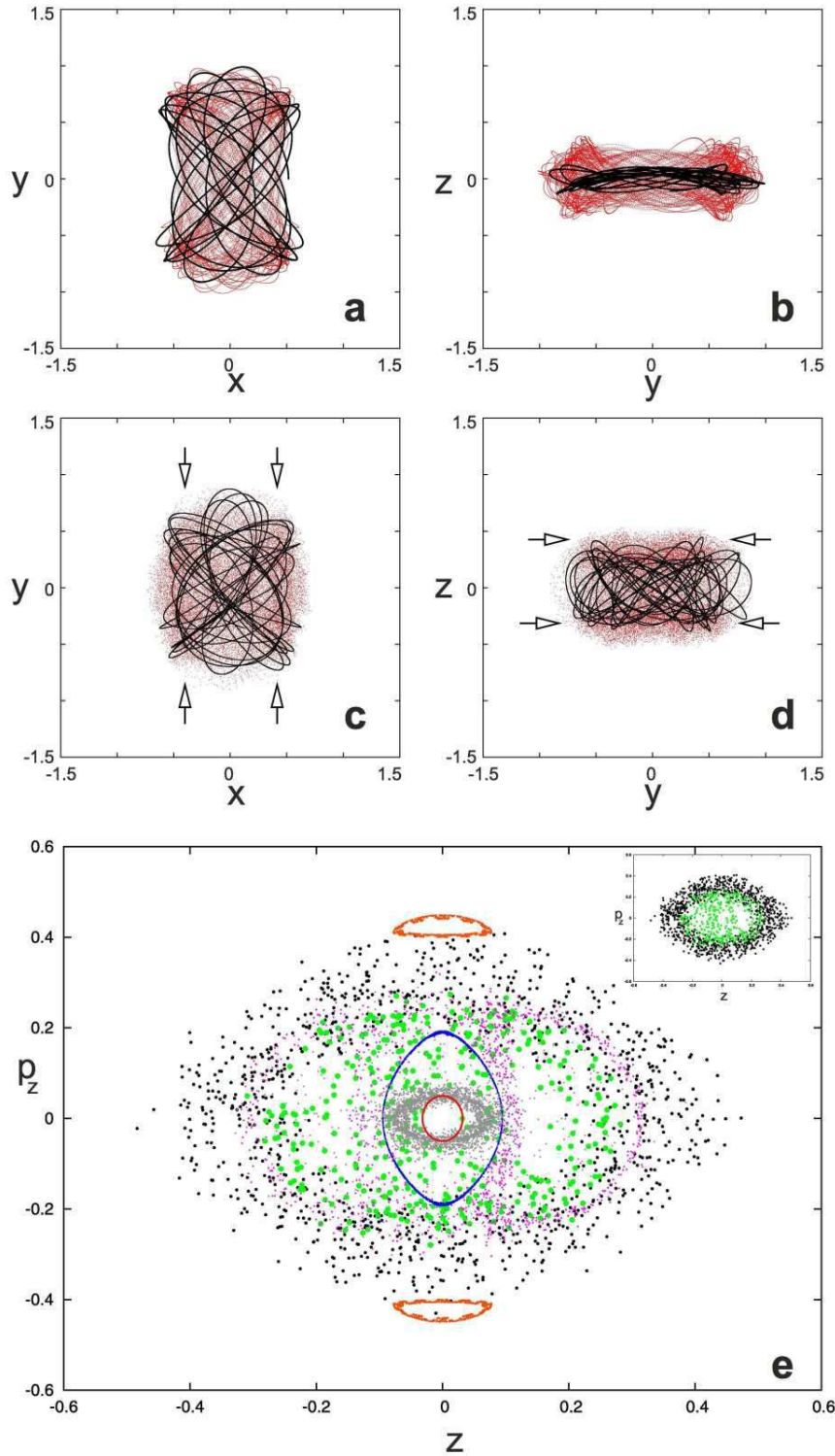


**Figure 8.** Contribution to boxy structures by an orbit with consequents projected in the chaotic zone of Fig. 1 ( $E_J = -0.41$ ). In (a) and (b) we give the face-on and side-on views respectively of an orbit starting at  $(x_0, z_0, p_{x_0}, p_{z_0}) = (0.515, 0.034, 0, 0)$  during phase “A” (see text), which lasts for 300  $x1$  periods at the same  $E_J$ . With black we depict the orbit during the first 10  $x1$  periods. In (b) and (c) we give the corresponding projections during phase “B” (see text), in the course of the subsequent 700  $x1$  periods. In (e) we present the  $(z, p_z)$  plane of the consequents of this orbit. Green points correspond to phase “A”, while “black” to phase “B”, while the inner grey ring corresponds to a later phase, when the orbit becomes sticky to  $x4$ . The magenta dots are the consequents of a sticky orbit to the  $x1v1$  and  $x1v1'$  tori. The central red and blue rings are projections of  $x1$  tori. In the embedded frame we isolate the consequents of the orbit during phase “A” and “B”, so that it becomes evident that the consequents during phase “B” practically surround those during phase “A”. Axes and dimensions of the embedded frame are as for the main one in (e).

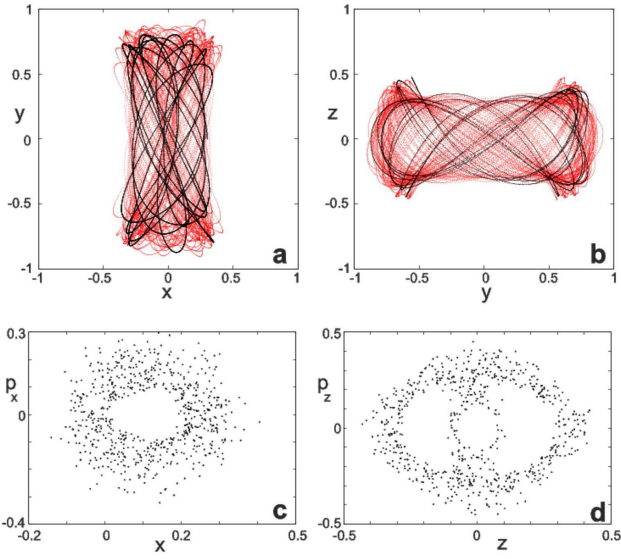


**Figure 9.** Typical morphologies of perturbed planar orbits with  $(x_0, p_{x_0})$  initial conditions in the central stability regions of Fig. 1. In (a) and (b) we give the face-on and side-on views respectively of an orbit starting at  $(x_0, z_0, p_{x_0}, p_{z_0}) = (0.3, 0, 0, 0.3)$  and integrated for 100  $x_1$  periods ( $E_J = -0.41$ ). In foreground with black we give the orbit during the first 10  $x_1$  periods. The  $(x, p_x)$  and  $(z, p_z)$  cross sections in (c) and (d) reproduce the characteristic imprint of orbits supporting a double boxy character.

the  $(x, p_x)$  and  $(z, p_z)$  projections of the consequents of the orbit of Fig. 9a,b. They are given in Fig. 9c,d. Especially in the  $(z, p_z)$  projection (Fig. 9d) it is clear that the orbit reproduces the pattern of the sticky orbits we have first encountered in figure 14 of paper I. The advantage of these orbits with respect to other orbits reinforcing the double boxy profiles is that one obtains this morphology immediately after starting integrating them without any delay.

## 2.2 Dynamics in the vILR region

In paper I we designated the energy interval in which  $x_1$  becomes simple unstable at the vertical ILR as  $\Delta E_{vILR}$ . Unlike the typical case with  $E_J = -0.41$  we used to discuss the dynamical mechanism in the previous section, in this interval  $x_1$  is not stable, but simple (vertically) unstable. Nevertheless, in the  $(x, p_x)$  plane we encounter around  $x_1$  invariant curves. We find that if we perturb in the vertical direction orbits on these invariant curves we may encounter again boxy face-on projections in the configuration space. The main reason for this is again the proximity of the  $x_1 v_1$  and  $x_1 v_1'$  tori to the initial conditions of  $x_1$ . There is always a  $\Delta z$  or  $\Delta p_z$  range for which the perturbed planar orbits are affected by the presence of these tori. The examples used in paper I for discussing vertically unstable  $x_1$  orbits, having 2D regular orbits around them in the  $(x, p_x)$  plane, are typical cases of such orbits. The perturbed by  $\Delta z = 0.02$   $x_1$  orbit at  $E_J = -0.438225$ , has a peanut shape side-on morphology (figure 5d of paper I). Its face-on view is a typical  $x_1$  ellipse with a negligible thickness (Fig. 10a). If we include  $\Delta x$  perturbations in this orbit and we start increasing them, the  $(x, y)$  projections of the resulting orbits in the beginning are thick ellipses. For  $x_0 \gtrsim 0.14$  (keeping always  $z_0 = 0.02$ ) their face-on projections have a clear boxy character (Fig. 10b). This boxiness increases with increasing  $x_0$ . For  $x_0 > 0.19$  the face-on view of the orbits are as for the orbit in Fig. 10c, for which  $x_0 \approx 0.29$ . The face-on morphology is boxy for all orbits starting with  $x_0 \approx 0.29$ ,  $p_x = 0$  and

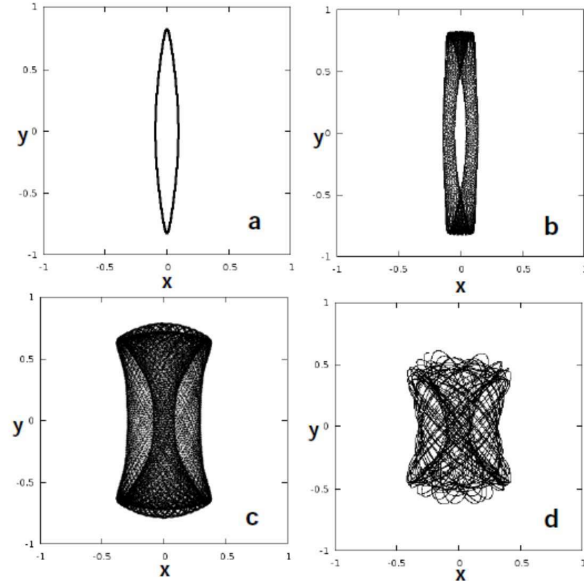


**Figure 10.** The evolution of the face-on projections of vertically perturbed orbits in the energy interval in which  $x_1$  is simple unstable. All four orbits are for  $E_J = -0.438225$ . (a) The perturbed by  $z = 0.02$   $x_1$  orbit. (b) The perturbed by the same  $\Delta z$  orbit with  $(x_0, p_{x_0}, p_{z_0}) = (0.14, 0, 0)$ . In (c) we increase the  $x_0$  initial condition of the orbit in (b) to  $x_0 = 0.29$  and in (d) we increase the  $z_0$  initial condition of the orbit in (c) to  $z_0 = 0.25$ .

$0.01 < z_0 < 0.26$ . We give the orbit with  $z_0 = 0.25$  in Fig. 10d (the orbits increase their projections on the  $x$ -axis as  $z_0$  increases). It is worth noticing that despite being double-boxy (in face-on and side-on views), and despite their similarity in their face-on projections, the orbits in Fig. 10b, 10c and 10d, have different boxy morphologies in their side-on views. The orbit in Fig. 10b has a shape like the one we have seen in figure 5d of paper I. The side-on morphologies of the orbits in Fig. 10c and Fig. 10d are similar to other profiles we encountered in paper I (see figures 6a and 6b respectively).

All these findings clearly show that there is a class of non-periodic orbits, either quasi-periodic or (especially) sticky to quasi-periodic orbits, that reinforce simultaneously boxy side-on and face-on profiles in our model. Such orbits with energies from the radial and vertical ILR region of our model give in their  $(x, y)$  projections boxy orbits that reach distances about 1 kpc from the centre along the  $y$ -axis. For larger energies, especially for  $E_J > -0.3$ , when  $x_1 v_1$  becomes again stable and other p.o. of the  $x_1$ -tree are introduced in the system, we find anew non-periodic orbits trapped by  $x_1 v_1$  tori. Such orbits may have a double boxy character, but remain narrow and do not participate to the building of the peanut. For example  $x_1 v_3$  or  $x_1 v_5$  orbits perturbed by  $z$  or  $p_z$  can give orbits with boxy face-on profiles, which however remain in small heights. These are orbits associated with a possible outer boxiness of the bar.

## 3 POSSIBLE CONTRIBUTION FROM ORBITS BIFURCATED AT ODD RESONANCES

As it is known (e.g. Contopoulos & Grosbøl 1989) in rotating galactic potentials, at the radial  $n:1$  resonances with  $n$  being an odd integer, we have a type 3 bifurcation (Contopoulos 2004, section 2.4.3). In that case, pairs of symmetric families are introduced in

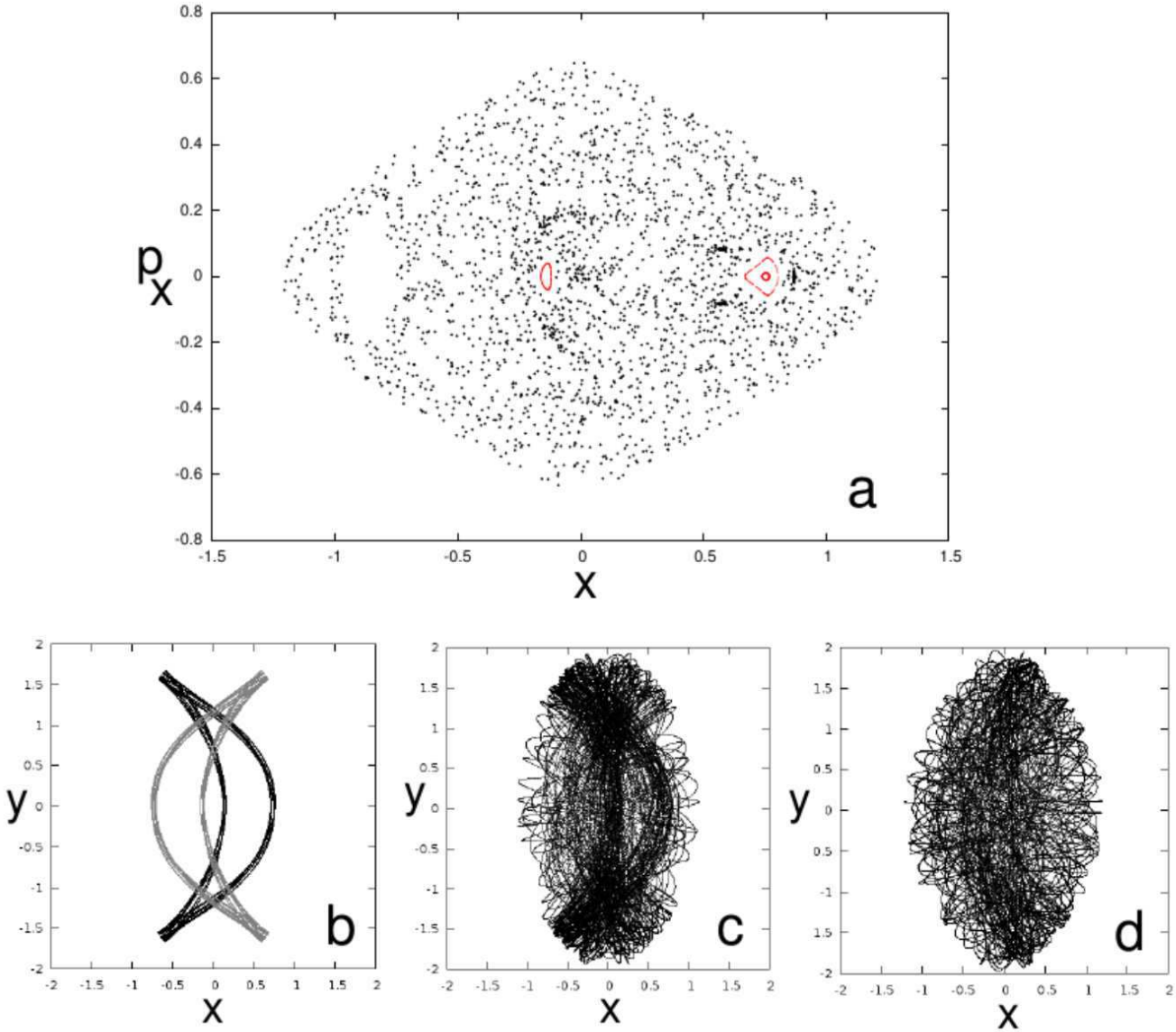


**Figure 11.** (a) A  $(x, p_x)$  Poincaré section at  $E_J = -0.35$  constructed by perturbing the initial conditions of  $o1$  by  $\Delta x$ . The two small stability islands are around  $o1$  ( $x > 0$ ) and  $o1'$  ( $x < 0$ ). (b) The  $(x, y)$  projection of two quasi-periodic orbits around  $o1$  and  $o1'$ . (c) A set of 13 sticky orbits with  $z_0 = 0.2$  and  $-0.2 < x_0 < 1.0$  (d) A set of 10 sticky orbits with  $p_{z_0} = 0.1$  and  $-0.105 < x_0 < 0.94$ . The rest of the initial conditions in all cases are 0. All orbits are integrated for 10  $o1$  periods.

the system. Usually we encounter such families as bifurcations of  $x1$  at the 3:1 radial resonance. By plotting together both branches of the symmetric periodic orbits belonging to the same family we create boxy features, as indicated by Patsis et al. (2003). Recently, Contopoulos & Harsoula (2014) have presented chaotic orbits in the neighbourhood of 3:1 p.o. that reinforce boxy morphologies close to the end of the bar if integrated for long times. However, for the inner boxiness we study here, the appropriate orbits have to support boxy features in the bar. In other words their  $(x, y)$  projections they have to lie inside the region occupied by the corresponding projections of the 3D orbits that support the peanut in the side-on view.

In our model the 3:1 families are bifurcated close to the end of the bar. Due to their dimensions, possible reinforcement of boxy

features by these orbits will be associated boxiness at  $y > 2$ . Also in the case of the potential from an  $N$ -body simulation studied by Contopoulos & Harsoula (2014), such orbits contribute to the outer boxiness of the bar. However, we have in our model another pair of planar symmetric families, of 1:1 resonance type, which are found in the right energy range. These orbits, called  $o1$  and  $o1'$ , are two branches of a family bifurcated as stable from  $x1$  at  $E_J = -0.38$ . They are discussed in Skokos et al. (2002b) and have a triangular type morphology. By considering both stable symmetric branches of  $o1$  (see figure 17 in Skokos et al. 2002b) we construct a skeleton that could support a boxy feature. In the interval  $-0.38 < E_J < -0.338$ ,  $o1, o1'$  are stable,  $x1$  is (radially) simple unstable,  $x1v1/x1v1'$  are complex unstable and  $x1v3$  is simple unstable. Fig. 11a shows a  $(x, p_x)$  Poincaré section for  $E_J = -0.35$

constructed by perturbing the initial conditions of  $o1$  by  $\Delta x$ . We observe a main chaotic sea with two stability islands belonging to  $o1$  ( $x > 0$ ) and  $o1'$  ( $x < 0$ ). There is an increased density of consequents around the islands, indicating the existence of sticky zones. We followed again the procedure of perturbing initial conditions on the  $(x, p_x)$  plane by  $\Delta z$  or  $\Delta p_z$ . We integrated them for time equal to 10  $o1$  periods. We found that the quasi-periodic orbits trapped by either of the symmetric branches of  $o1$  have morphologies similar to those of the p.o. when projected on the  $(x, p_x)$  plane, but are thicker. The orbits in Fig. 11b are the quasi-periodic orbits we obtain by perturbing  $o1$ ,  $o1'$  by  $\Delta z = 0.1$ .

Starting from the p.o., or from initial conditions on an invariant curve around  $o1/o1'$ , or even from a  $(x, p_x)$  point belonging to a sticky zone, we find sticky orbits when exceeding a critical  $\Delta z$  or  $\Delta p_z$  perturbation. Typical examples are given in Figs. 11c and 11d. In Fig. 11c we plot 13 orbits with  $(x_0, p_{x0}, z_0, p_{z0}) = (-0.2 < x_0 < 1.0, 0, 0.2, 0)$ , while in Fig. 11d 10 orbits with  $(x_0, p_{x0}, z_0, p_{z0}) = (-0.105 < x_0 < 0.94, 0, 0, 0.1)$ . Most of these orbits are sticky to  $o1$  and  $o1'$ . We observe that the boundary of these orbits has an oval shape. Combining sticky orbits we do not find symmetric morphologies in general, even if we perturb by equal  $\Delta z$  or  $\Delta p_z$  the initial conditions of the periodic orbits. Non-periodic orbits associated with the  $o1/o1'$  family fail to provide clear boxy features in their face-on views like the orbits in Figs. 8, 9 and 10. By comparing the phase space in the case of the latter orbits with that of the orbits in Fig. 11, we observe that the main difference is the lack of the rotational tori around  $x1v1$  and  $x1v1'$ . When  $o1$  is introduced in the system  $x1v1$  and  $x1v1'$  are already complex unstable. This indicates that the main dynamical phenomenon for having boxiness in the middle of the bar is stickiness to these tori. In other models in which 3:1 type families exist at the energies we have stable  $x1v1$  and  $x1v1'$  orbits they may play a role similar to that of  $rm2$  and  $tr1$  in Figs. 1 and 8.

#### 4 DISCUSSION AND CONCLUSIONS

Summarizing we can say that as long as a non-periodic orbit in the radial and vertical ILR region of our model is trapped by, or becomes sticky to,  $x1v1$  and/or  $x1v1'$  tori, it may visit a region of phase space, where the orbits have rectangular-like face-on  $(x, y)$  projections. Rectangularity in the morphology of non-periodic orbits is evidently related with the presence of 2D families of p.o. with boxy shapes in the equatorial plane. The presence of families like  $rm21$ ,  $rm22$  and  $tr1$  in  $(x, p_x)$  cross sections indicate the prevalence of boxy shapes in large regions of the phase space over a large energy interval. Inner boxiness is generated by perturbing initial conditions of planar orbits at energies where we find orbits with rectangular shapes on the equatorial plane and  $x1v1/x1v1'$  tori in the phase space. As a result the orbits participating in the inner boxiness have a double boxy character (face-on and edge-on). Among them those that reach larger heights above the equatorial plane tend to become more square.

Boxy periodic orbits of higher multiplicity facilitate the prevalence of boxy morphologies, because they influence larger regions of the phase space. In a typical case we have small stability islands with larger sticky zones around them. Sticky chaotic orbits visit phase space regions that are far from each other. Planar families of symmetric p.o. introduced at odd radial  $n:1$  resonances do not play an important role for the inner boxiness in our model. However, they can be significant in models where they co-exist in the same energy intervals with the tori of  $x1v1$  and  $x1v1'$ .

In Fig. 12 we put together representative non-periodic orbits that support double boxy profiles, both from the 2:1 resonance region as well as from regions of higher resonances. The outermost, thicker drawn, black orbit, discernible in Figs. 12a and b, is a  $x1v6$  orbit that we identify with the longest bar-supporting p.o. and is used as a measure of the length of the bar in our model. The longest boxy orbit in Fig. 12a, drawn with magenta colour is at  $E_J = -0.254$ . In Fig. 12b, which is an almost side-on view of the same set of orbits, we can see the same magenta coloured orbit remaining in much lower heights than the orbits that build the peanut. Its detailed shape, hidden by the other orbits in the central regions of the model, points to an association with  $x1v3$ . By converting Fig. 12a to an image and by applying a smoothing filter, we obtain Fig. 12c. We can observe how inner and outer boxiness can be formed in our model by means of quasi-periodic and sticky orbits. It has to be underlined that orbits at higher energies participating in the formation of the “X-feature” in the side-on views, especially by means of orbits associated with the  $x1v1$  and  $x1v1'$  families, contribute in general less to the surface density of the central parts of the face-on views of the bars and more to their periphery, as long as they retain a clear loop character. The closer the “X” supporting non-periodic orbits remain trapped around the  $x1v1$  and  $x1v1'$  periodic orbits, the larger is the “transparency” towards the face-on rectangular-like periodic orbits at lower energies with smaller heights above the equatorial plane. This becomes evident in Fig. 13 by means of a set of quasi-periodic orbits with  $E_J = -0.27$ . Two are trapped around  $x1v1$  and  $x1v1'$  (coloured red), while the other two (coloured black) have boxy face-on projections and are from the  $\Delta E_{vILR}$  energy interval. In (a) we have a nearly side-on and in (b) the face-on view. We observe that the outer (red) orbits have also a rectangular-like face-on character, although not as boxy as the inner two.

In Erwin & Debattista (2013) it is presented a list with 30 galaxies (see their A1, A2 figures) with boxy isophotes in the middle of the bar. These are moderately inclined galaxies, far from edge-on. Since the bar of our model does not contain asymmetric terms, it is aligned with the major axis of the system. So the extent and the proportions of the inner and outer boxiness in the face-on views of the bar can be compared with rather symmetric galactic bars, in galaxies with inclinations  $i < 50^\circ$  like the one of NGC 4037 or NGC 4123 (see figures with isophotes in Erwin & Debattista 2013).

The main conclusions of our study are:

(i) The *inner* boxy isophotes in the middle of the bars in nearly face-on views of barred galaxies can be supported by 3D quasi-periodic and mainly by 3D chaotic orbits sticky to  $x1v1$  and  $x1v1'$  p.o. in the ILR region. Inner boxiness is also characterized by the presence of planar periodic orbits with boxy morphology at the appropriate energies. By perturbing vertically such p.o. we generate a class of non-periodic orbits with double boxy character. The maximum distance along the bar’s major axis reached by these orbits is at or inside the limits of the b/p bulge. Higher multiplicity p.o. influence large regions of the phase space, mainly due to the presence of sticky zones around their stability islands. Orbits sticky to multi-periodic orbits have consequents in the sticky zones around different islands. This way a boxy structure can be supported by orbits with initial conditions in regions of the phase space that are far from each other.

(ii) At large energies, orbits that reinforce “X-features” in the side-on views of b/p bulges by staying close to the periodic orbit, enhance locally boxy face-on features without obscuring the sight

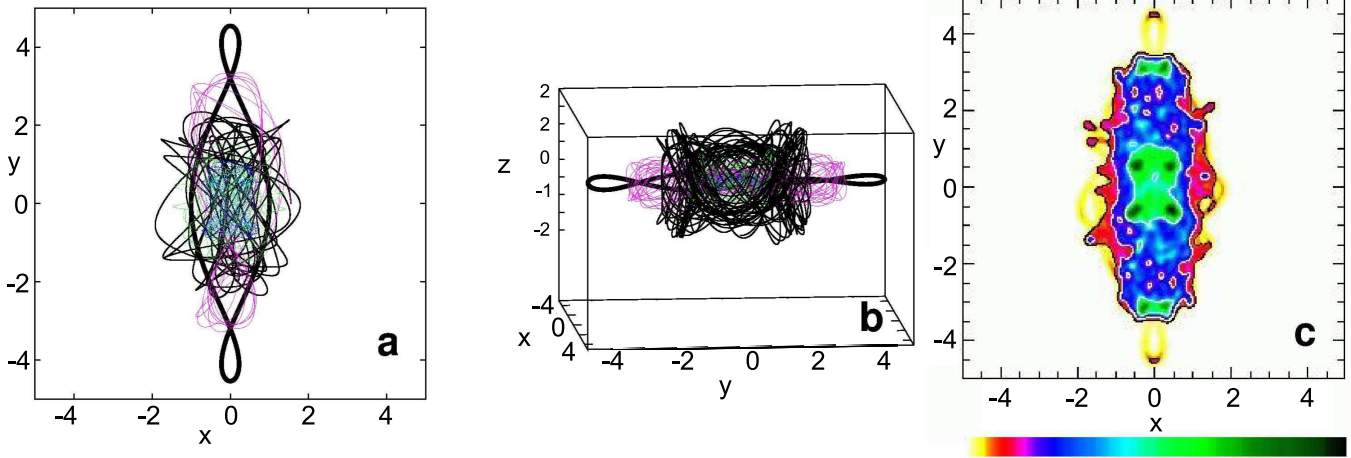


**Figure 12.** A set of representative non-periodic orbits that support double boxy profiles. (a) The face-on and (b) a nearly side-on view of these orbits. In (c) we apply a smoothing filter on an image based on the orbits in (a) to indicate the boxy features reinforced in the model.

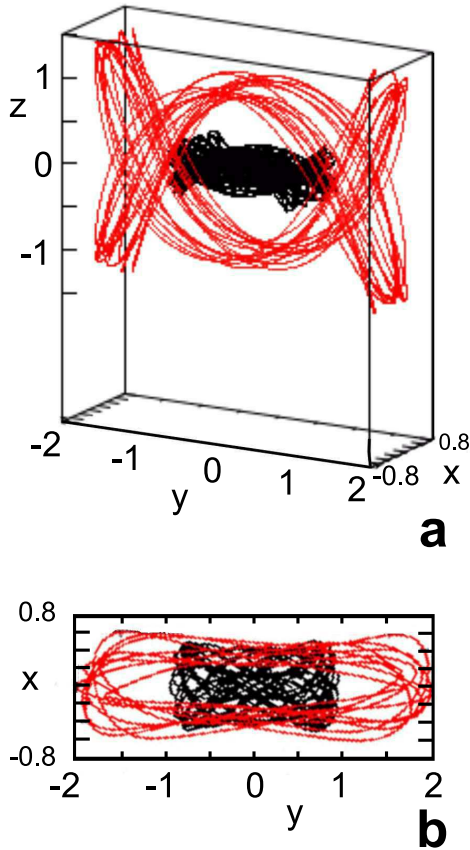


**Figure 13.** Two sets of orbits supporting the “X-feature” having boxy face-on projections both in a nearly side-on (a) as well as in their face-on view (b). The trapping of quasi-periodic orbits close to  $x1v1$  and  $x1v1'$  p.o. at the outer part of the b/p bulge (coloured red) facilitates the observation of structures supported by orbits in lower heights (coloured black) in the face on views of the model.

towards boxy structures formed at lower heights. The latter are located closer to the centre of the galaxies in the  $(x, y)$  projections.

(iii) Boxiness at the outer parts of the bars is supported by orbits associated with families of higher resonances of the  $x1$ -tree, which remain very close to the equatorial plane.

#### Acknowledgements

We thank Prof. G. Contopoulos for fruitful discussions and very useful comments. This work has been partially supported by the Research Committee of the Academy of Athens through the project 200/815.

#### REFERENCES

- Contopoulos G., 1983, *ApJ* 275, 511  
 Contopoulos G., 1988, *A&A* 201, 44  
 Contopoulos G., 2004, “Order and Chaos in Dynamical Astronomy”, Springer Verlag, Berlin-Heidelberg  
 Contopoulos G., Harsoula M., 2013, *MNRAS* 436, 1201  
 Contopoulos G., Grosbøl P., 1989, *A&AR*, 1,261  
 Erwin P., Debattista V.P., 2013, *MNRAS* 431, 3060  
 Katsanikas M., Patsis P.A., 2011, *Int. J. Bif. Ch.* 21-02, 467  
 Kaufmann D., Contopoulos G., 1996, *A&A* 309, 381  
 Ohta K., Hamabe M., Wakamatsu K., 1990, *ApJ* 357,71  
 Patsis P.A., 2006, *MNRAS* 369L, 56  
 Patsis P.A., Katsanikas M., 2014, *MNRAS* (in Press)  
 Patsis P.A., Athanassoula E., Quillen A.C., 1997, *ApJ* 483, 731 2  
 Patsis P.A., Skokos, Ch., Athanassoula E., 2003, *MNRAS* 342, 69  
 Poincaré H., 1899, ‘Les Methodes Nouvelles de la Mechanique Celeste’, Vol III, Gauthier-Villars, Paris  
 Skokos Ch., Patsis P.A., Athanassoula E., 2002a *MNRAS* 333, 847  
 Skokos Ch., Patsis P.A., Athanassoula E., 2002b *MNRAS* 333, 861  
 Tsigaridi L., Patsis P.A., 2013, *MNRAS* 434, 2922  
 Vrahatis M., Isliker H., Bountis T.C., 1997, *Int. J. Bif. Ch.* 7, 2707  
 Wozniak H., 1994, in “Ergodic Concepts in Stellar Dynamics”,

LNP 430, 264, V. G. Gurzadyan & D. Pfenniger (eds), Springer-Verlag, Berlin Heidelberg New York  
Wozniak H., Pfenniger D., 1999, *Cel. Mech. Dyn. Ast.*, 73, 149